Journal of Power Sources 185 (2008) 480–485

Contents lists available at ScienceDirect

Journal of Power Sources

journal homepage: www.elsevier.com/locate/jpowsour

Composite effect in superionically conducting lithium aluminium germanium phosphate based glass-ceramic

Joykumar S. Thokchom *, Binod Kumar

Electrochemical Power Group, Metals and Ceramics Division, University of Dayton Research Institute, Dayton, OH 45469-0170, USA

ARTICLE INFO

Article history:
Received 20 June 2008
Received in revised form 7 July 2008
Accepted 9 July 2008
Available online 17 July 2008

Keywords:
Glass-ceramic
Crystal structure
Microstructure
Superionic conductivity
Heterogeneity
Space charge effect

ABSTRACT

Superionically conducting lithium aluminum germanium phosphate (LAGP) glass-ceramic and barium strontium titanate, $Ba_{0.6}Sr_{0.4}TiO_3$ (0.6BST)-doped specimens were processed and characterized using X-ray diffraction (XRD), scanning electron microscopy (SEM), and AC impedance techniques. The XRD patterns exhibited the existence of $LiGe_2(PO_4)_3$ as the primary phase with impurity phases $AlPO_4$ and Li_2O. SEM images revealed the presence of large LAGP crystals. The highest conductivity (5.08×10^{-3} S cm^{-1}) at 27 °C was obtained for the glass-ceramic sheet specimen crystallized at 850 °C for 12 h. Pelletized specimens prepared from the glass-ceramic powder and sintered at 850 °C for 9 h exhibited a slightly lower conductivity (4.62×10^{-3} S cm^{-1}) at 27 °C. The nonlinearity in the Arrhenius plots of total conductivity was attributed to the impurity phases, $AlPO_4$ and Li_2O and mediated the transport of lithium ion which is associated with higher activation energy. Doping of dielectric 0.6BST to the LAGP led to the shifting of the temperature of inflection towards the higher temperature in the Arrhenius plot of total conductivity and enhanced the space charge effect.

1. Introduction

In the current scenario of worldwide increases in gasoline prices and the depletion of petroleum resources, the need to explore alternative portable and stationary power sources based on lithium batteries has become essential to support and sustain the global economy, electronics technology, and a clean environment. In last decade, some progress has been made in lithium technology. Existing commercial lithium batteries use graphite or nano-lithium titanate as anode and mixed metal oxide or phosphate as cathode sandwiching the liquid electrolyte-soaked separator. However, problems with electrodes and liquid-related safety issues have been encountered for these batteries.

In recent times, researchers have envisioned developing all solid-state lithium batteries with higher energy and power density capabilities by deploying lithium metal as fuel in the form of anode and other variants of the advanced batteries [1,2]. Lithium metal as anode material is highly attractive as it has the highest gravimetric capacity (3800 Ah kg^{-1}). The lack of mechanically robust solid materials with a high ambient temperature conductivity ($\geq 1 \times 10^{-3}$ S cm^{-1}), large cationic transport number, compatibility with potential electrodes, electrochemical stability window, and ease of processing into useful shapes are drawbacks to realizing these possibilities. Further, such materials possess the potential for developing the highest power density lithium chemistries such as lithium–air and lithium–water batteries.

Ever since the development of ceramic ionic conductors based on a $LiM_2N_{2-x}(PO_4)_3$, M = Al, Sc, Y, La; N = Ti, Ge, Hf, Sr structure, which is analogous to a NASICON-type structure [3,4], relentless research on this promising group of oxide-based solid lithium ion conductors has mainly focused on substituents like Ti or Ge or both. Aono et al. [3] reported a conductivity of 7×10^{-4} S cm^{-1} at 25 °C for a $Li_{1.3}Al_{0.3}Ti_{1.7}(PO_4)_3$ (LATP) pellet specimen with 6% porosity. Adachi et al. [5] compared and contrasted the ionic conductivity and mechanical properties of various solid lithium ion conductors with promising potential for LATP material. Fu [6,7] reported the room temperature conductivity values for the $Li_{1.3}Al_{0.3}Ti_{1.7}(PO_4)_3$ and $Li_{1.5}Al_{0.5}Ge_{1.5}(PO_4)_3$ glass-ceramic materials obtained by crystallization at 950 and 822 °C for 12 h each to be 1.3×10^{-3} and 4×10^{-4} S cm^{-1}. Chowdari et al. [8] reported bulk conductivities of $Li_{1.3}Al_{0.3}Ti_{1.7}(PO_4)_3$ and $Li_{1.4}Al_{0.4}Ge_{1.6}(PO_4)_3$ glass-ceramic materials to be 6.53×10^{-4} and 3.99×10^{-4} S cm^{-1} at 30 °C. These Ti- and Ge-based systems were heat treated at 950 and 750 °C, respectively, for 12 h. Xu et al. [9] prepared the $Li_{1.4}Al_{0.4}(Ge_{0.67}Ti_{0.33})_{1.6}(PO_4)_3$ glass and crystallized at 950 °C for a longer period (18 h) to obtain glass-ceramic materials that showed a maximum room temperature conductivity of 6.21×10^{-4} S cm^{-1}. In another paper, Xu et al. [10] reported higher conductivity

* Corresponding author. Tel.: +1 937 229 4355; fax: +1 937 229 3433.
E-mail address: joykumar.th@notes.udayton.edu (J.S. Thokchom).

0378-7753/$ – see front matter © 2008 Elsevier B.V. All rights reserved.
doi:10.1016/j.jpowsour.2008.07.009

(1.09×10^{-3} S cm^{-1}) in a similar material. The specimen was prepared by mechanically milling nano-sized $Li_{1.4}Al_{0.4}Ti_{1.6}(PO_4)_3$ glass-ceramic and subsequently sintering a pressed specimen at 900 °C for 6 h. High conductivity glass-ceramic material based on the Li_2O–Al_2O_3–TiO_2–P_2O_5 system primarily consisting of $Li_{1+x}Ti_{2-x}Al_x(PO_4)_3$ ($x \sim 0.3$) phase—a derivative of the $LiTi_2(PO_4)_3$ structure was also prepared, characterized, and reported by Thokchom and Kumar [11].

It is critical that the solid electrolytes used for fabricating the lithium batteries must be in stable in contact with the anode materials like lithium metal. The superior stability of the lithium aluminum germanium phosphate (LAGP) material in contact with lithium metal has been reported in the literature [12,13]. Therefore, based on the ionic conductivity and interfacial stability, the LAGP material is very attractive for fabricating cells with superior electrochemical performance.

In heterogeneous solid ionic conductors, an ionic conducting matrix contains a second dielectric phase, thus forming a composite. Prior investigations [14–16] have explained the effect of the dielectric phase on conductivity in terms of space charge and/or blocking effects. The space charge has a major influence on the transport of conducting ions and enhances conductivity of ionic solids under appropriate conditions. Collectively, these factors determine whether or not a given dopant will have a positive space charge effect i.e., an enhancement in conductivity with the addition of the dopant. Maier [17] developed the theory of ionic conduction in heterogeneous solids highlighting the importance of space charge regions or phase boundaries. Furthermore, space charge signature and its effect on the ionic transport in heterogeneous solids has been reported in the literature [18].

The present work reports the processing and characterization specifically crystal structure, ionic conductivity, and microstructure of a LAGP glass-ceramic material <1 mm thick that possesses a liquid-like ionic conductivity (5.08×10^{-3} S cm^{-1}) at 27 °C. The effect of sintering time and composite effect on conductivity due to the doping of a high dielectric material (barium strontium titanate, 0.6BST) are also discussed.

2. Experimental

2.1. Melting and crystallization

A glass batch [$19.75Li_2O{\cdot}6.17Al_2O_3{\cdot}37.04GeO_2{\cdot}37.04P_2O_5$ (mol%)] comprised of reagent grade chemicals such as Li_2CO_3 (Alfa Aesar), Al_2O_3 (Aldrich, particle size <10 μm), GeO_2 (Acros Organics), and $NH_4H_2PO_4$ (Acros Organics) was prepared. The aforementioned chemicals were weighed, mixed and milled in a glass jar for 1 h. The milled batch in a platinum crucible was melted in an electric furnace. Initially, the furnace was heated to 450 °C at the rate of 0.5 °C min^{-1} and held at that temperature for 1 h to release the volatile batch components before raising the furnace temperature to 1350 °C at the rate of 1 °C min^{-1} after which the glass was melted for 2 h. A clear, homogeneous, viscous melt was poured onto a preheated (~200 °C) stainless steel plate and pressed by another steel plate to yield <1 mm thick transparent glass sheets. Subsequently, the cast and pressed glass sheets were annealed at 500 °C for 2 h to release the thermal stresses and then furnace cooled. These annealed specimens remained in the glassy state. The annealed glass was subsequently crystallized at 850 °C for 12 h and at 950 °C for 6 h, respectively. This crystallization transformed the glass to crystalline ceramic, also known as glass-ceramic, that possesses a very high ionic conductivity. A change in the appearance of the glass from colorless, transparent to bluish opaque was also observed after the crystallization. Further, the glass-ceramic sheets were crushed into chunks, powdered, and screened to obtain the powder of <38 μm size. About 200 mg of the powder was used to prepare ~1 mm thick pellets of ~12.68 mm diameter by pressing with pressure of 690 MPa. The pellets were sintered at 850 °C for 3, 6, 9, and 12 h to obtain the specimens. Similarly, LAGP-0.6BST composite specimens with different vol% doping of 0.6BST were prepared for characterization.

2.2. Thermal studies

Differential scanning calorimeter measurement was carried out on MDSC 2920 (TA Instruments, USA) in standard mode. 10 mg piece of LAGP glass specimen was used for the DSC recording. The specimen was placed on a gold pan while an empty gold pan was used as a reference. The sample was heated to 725 °C from room temperature at the rate of 10 °C min^{-1}. During the measurement dry nitrogen gas was used to purge the DSC sample cell at the rate of 50 cc min^{-1}.

2.3. X-ray diffraction

X-ray diffraction (XRD) patterns for LAGP glass-ceramic specimens crystallized at 850 °C for 12 h and 950 °C for 6 h were recorded using a Rigaku Rotaflex RV-200BH X-ray diffractometer operated at 40 kV, 150 mA current with a copper target in the 2θ range of 10–80° at 0.05° increments.

2.4. Scanning electron microscopy

Microstructure investigations were conducted on bulk glass-ceramic and also on sintered specimens obtained by compacting glass-ceramic powder and subjecting it to a sintering heat treatment at 850 °C for 12 h using a high resolution scanning electron microscope (Hitachi S-4800 HRSEM; Hitachi High Technologies America, Inc., Pleasanton, CA). Thermal etching of the polished specimens was carried out at 650 °C for 3 h.

2.5. AC impedance measurements

The AC impedance measurements on a glass-ceramic sheet specimen crystallized at 850 °C for 12 h, pelletized glass-ceramic specimens sintered at 850 °C for 3, 6, 9, and 12 h, and LAGP glass-ceramic doped with different vol% of 0.6BST dielectric material were carried out using a Solartron instrument (Model 1260 with an electrochemical interface; Solartron US, Houston, TX) in the 0.01 to 10^6 Hz frequency range. An approximately 0.5 μm thick gold coating was sputtered on both sides of these specimens. The gold-coated sheet and disc specimens were assembled into a cell using stainless steel blocking electrodes in a cell fixture. The fixture containing the SS/electrolyte/SS cell was subsequently placed in a stable fixture holder with attached electrical wires leading to the impedance spectrometer. The AC impedance of the electrolyte was measured in the −42 to 127 °C temperature range. At each temperature, the specimen was equilibrated for 1 h before the impedance was measured. The specimen conductivity was computed from the AC impedance spectra. Z Plot and Z View softwares was used for data acquisition and analysis.

3. Results and discussion

3.1. Thermal properties

The DSC curve for as-cast LAGP glass is shown in Fig. 1. LAGP glass exhibited a distinct and strong exothermic crystallization peak, T_c, at around 637 °C with a glass transition temperature, T_g,

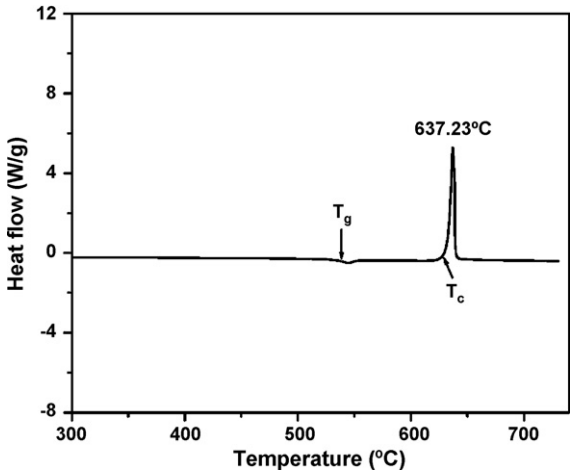

Fig. 1. DSC plots of as-cast LAGP glass specimen.

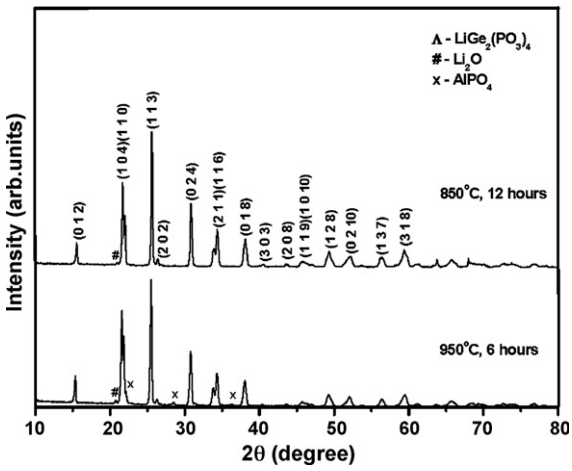

Fig. 2. XRD plots of LAGP glass-ceramic sheet specimens crystallized at 850 °C for 12 h and 950 °C for 6 h.

at around 538 °C. The exothermic peak is attributed to the crystallization temperature, T_c. The estimated T_g and T_c values match very well with the corresponding values reported for the similar composition and heat treatment [7].

3.2. Crystal chemistry and structure

A comparative analysis of molar compositions of the batch formulation ($19.75Li_2O{\cdot}6.17Al_2O_3{\cdot}37.04GeO_2{\cdot}37.04P_2O_5$) and $Li_{1+x}Al_xGe_{2-x}(PO_4)_3$ sheet material obtained by crystallization at 850 °C for 12 h is presented in Table 1. From the extensive energy dispersive X-ray (EDX) studies, the average value for the P/Ge ratio in the crystalline phase was detected to be 2.03, which is in close agreement with the batched composition value of 2. If all aluminium replaces the germanium site in the lattice of $LiGe_2(PO_4)_3$ crystal, which is a justified assumption as they have similar ionic radii ($Ge^{4+} = 0.39^{IV}$, 0.53^{VI}, $Al^{3+} = 0.39^{IV}$, 0.54^{VI} Å), then the value of x in the $Li_{1+x}Al_xGe_{2-x}(PO_4)_3$ is equal to 0.5. This stoichiometry was further confirmed by the EDX analysis. Further, the existence of a Li_2O phase which is 1.23% greater than the minimum concentration needed to form the $Li_{1+x}Al_xGe_{2-x}(PO_4)_3$ ($x = 0.5$) is evident. Perhaps the Li_2O is concentrated in the grain boundary regions. From this analysis, it is inferred that $19.75Li_2O{\cdot}6.17Al_2O_3{\cdot}37.04GeO_2{\cdot}37.04P_2O_5$ glass crystallized at 850 °C for 12 h primarily consists of a mixture of $Li_{1.5}Al_{0.5}Ge_{1.5}(PO_4)_3$ and Li_2O phases.

Fig. 2 shows the XRD patterns for the glass sheet specimens crystallized at 850 °C for 12 h and 950 °C for 6 h. The diffraction peaks corresponding to $LiGe_2(PO_4)_3$ (LGP) and Li_2O phases are observed in the XRD pattern for the specimen crystallized at 850 °C for 12 h. The high conductive phase (LGP) precipitates the most with a negligible excess amount of Li_2O that peaks at 21° as also noticed in the above crystal chemistry analysis. The LAGP glass specimen crystallized at 950 °C for 6 h shows the presence of an $AlPO_4$ phase with peaks at 22°, 28° and 36°, however, the $LiGe_2(PO_4)_3$ phase is dominant in the pattern. Indices for the various peaks are also indicated in the figure. Hexagonal lattice parameters obtained for the LGP crystalline phase in both the specimens are $a = 8.25$ Å and $c = 20.46$ Å, respectively, and these values match exactly with the literature data for $LiGe_2(PO_4)_3$ crystal phase [PDF card #41-0034 and 35-0754]. Indexing of the peaks beyond 60° was not carried out due to the limitation in the PDF cards. Both of the secondary phases, Li_2O and $AlPO_4$, are considered to be concentrated in the grain boundary region. This analysis confirms that added Al^{3+} ions were incorporated into the structure by replacing Ge^{4+} ions.

3.3. Microstructure

The scanning electron micrographs of thermally etched and fractured surfaces of the glass-ceramic sheet specimen crystallized at 850 °C for 12 h and pellet specimen sintered at 850 °C for 9 h are shown in Fig. 3(a)–(d). The thermally etched surface micrograph for the sheet specimen shows a clear morphology of grains with a size range from 0.1 to 1 μm [Fig. 3(a)], whereas the microstructure of the pelletized glass-ceramic specimen shows a broader crystal size distribution ranging from 0.43 to 3 μm, Fig. 3(b). The grain size increased by 77% for the smallest grain and 67% for the largest grain. The larger crystal size for the pellet specimen could be explained by the fact that the specimen was subjected to an additional sintering heat treatment at 850° for 9 h, which allowed further growth of the major crystalline phase, $Li_{1+x}Al_xGe_{2-x}(PO_4)_3$. Comparison of micrographs for the fractured surface of the sheet and pellet specimens (Fig. 3(c) and (d)) reveals different fracture patterns. It is apparent that sheet has a combined inter- and trans-granular fracture pattern whereas pellet has only a trans-granular fracture mode. This difference in fracture mode can be attributed to the large increase in grain size and densified structure of the pellet specimen compared to the sheet specimen. The density values for the sheet and pellet specimens were found to be 3.12 and 3.26 g cm^{-3}. The pellet is approximately 4.3% denser than the sheet specimen.

Table 1
Comparative analysis of molar composition for the LAGP glass-ceramic specimen

	Mol% of formulated LAGP	$Li_{1+x}Al_xGe_{2-x}(PO_4)_3$ ($x = 0.5$)	Normalized (w.r.t. Al_2O_3, GeO_2, and P_2O_5) ($x = 0.5$)
Li_2O	19.75	18.75	18.52
Al_2O_3	6.17	6.25	6.17
GeO_2	37.04	37.50	37.04
P_2O_5	37.04	37.50	37.04
P/Ge ratio	2.00	EDX = 2.03	2.00

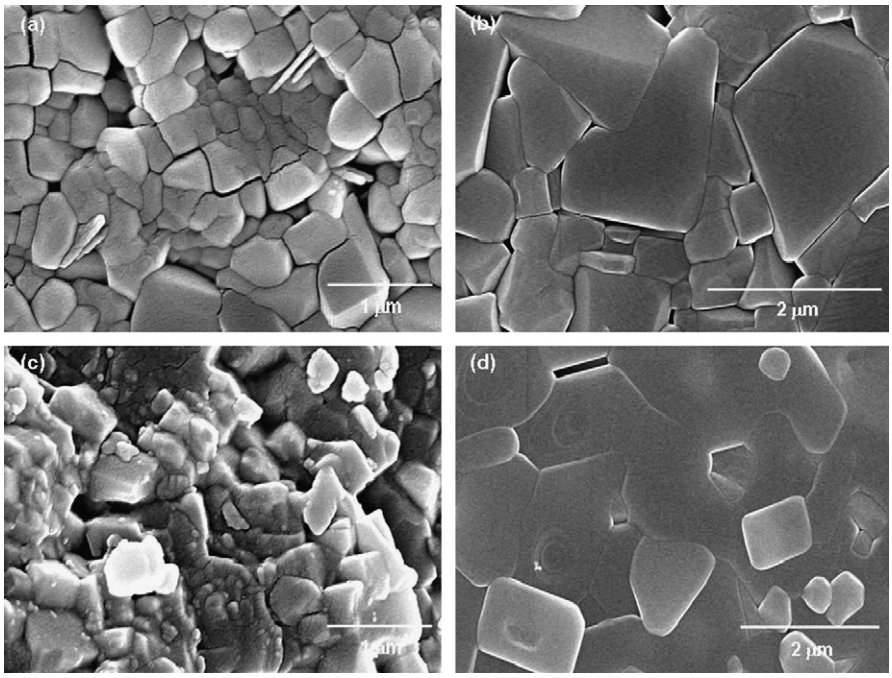

Fig. 3. Microstructures of (a) thermally etched and (c) fractured surfaces of the glass-ceramic sheet specimen crystallized at 850 °C for 12 h and (b) thermally etched and (d) fractured surfaces of the pelletized specimen sintered at 850 °C for 9 h.

The impurity phases, Li_2O and $AlPO_4$, are not visible in the micrographs, perhaps because their concentrations are small and are believed to be primarily segregated at the grain boundaries.

3.4. AC impedance and ionic conductivity

Room temperature AC impedance spectra of the sheet specimen crystallized at 850 °C for 12 h is shown in Fig. 4. The spectra show an intersection at the high frequency side of the Z'-axis, which is interpreted as circuit resistance external to the specimen. Starting from the intersection on the lower frequency side, a distorted semicircle representing grain and grain boundary resistances develops. The diameter of the semicircle is equal to the resistance of the specimen at the particular temperature, which is further normalized with respect to the thickness and cross-sectional area of the specimen to obtain the total conductivity, σ (S cm^{-1}). The impedance spectra reveal that the grain boundary contribution in total conductivity dominates the grain contribution.

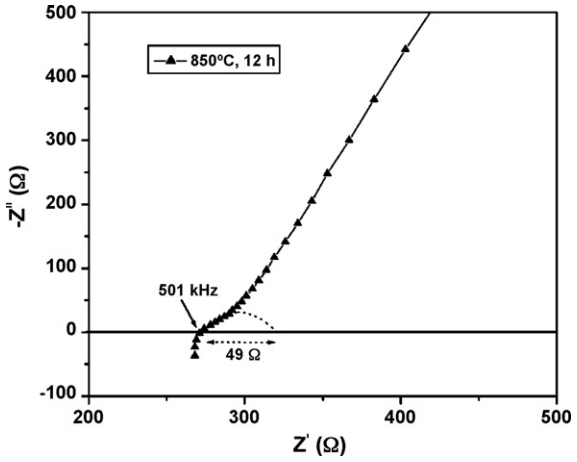

Fig. 4. Room temperature impedance spectra for LAGP glass sheet crystallized at 850 °C for 12 h.

Fig. 5 shows the Arrhenius total conductivity plots in the range of −42 to 107 °C of the sheet specimen which was crystallized at 850 °C for 12 h and pelletized specimens prepared using glass-ceramic powder and sintered for different times (3, 6, 9, and 12 h). The highest conductivity across the entire temperature range was associated with the sheet specimen crystallized at 850 °C for 12 h. The conductivity of the specimen ranged from 10^{-3} to 10^{-2} S cm^{-1} around the ambient temperature with a maximum value of 5.08×10^{-3} S cm^{-1} at 27 °C. The observed conductivity is about an order of magnitude higher than reported values [5,7], which can be attributed to the larger grain size and higher density of the LAGP material. Perhaps the presence of excess Li_2O in the LAGP system as detected in the X-ray diffraction data had the effect of achieving a denser LAGP material. This property of Li_2O was reported in the literature for similar systems [5]. Since the conductivity at 107 °C was

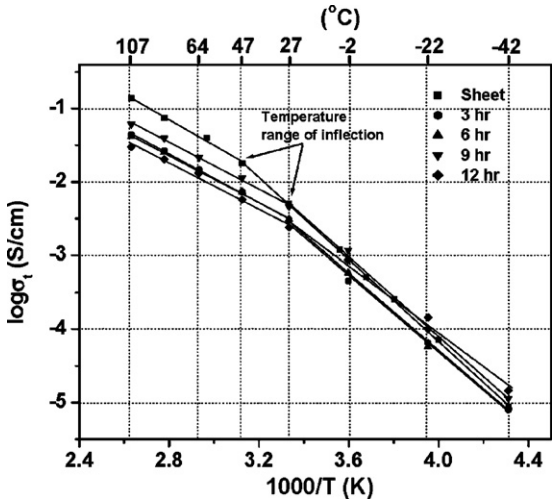

Fig. 5. Arrhenius plot of total conductivity for LAGP glass-ceramic sheet specimen crystallized at 850 °C for 12 h and pelletized specimens sintered at 850 °C for different hours.

over 100 mS cm^{-1}, the specimen can be described as a superionic conductor. The Arrhenius total conductivity plot of the specimen is nonlinear, constituting two linear segments intersecting at about 27–47 °C. However, each linear region fits the Arrhenius equation as expressed by:

$$\sigma = A \exp\left(\frac{-E_a}{kT}\right) \quad (1)$$

where A is the pre-exponential factor, E_a the activation energy, k the Boltzmann constant.

The nonlinearity is attributed to the presence of the impurity phases, $AlPO_4$ and Li_2O. The presence of the $AlPO_4$ phase in the glass-ceramic sheet specimen crystallized at 850 °C for 12 h was beyond the detectable level. However, its presence was observed for the specimen crystallized at a higher temperature (950 °C) as seen in the XRD pattern (Fig. 2). The properties of $AlPO_4$ are similar to SiO_2, and it is a dielectric. In a recent publication, Kumar [19] showed that dielectric dopants in an ionic conducting solid interact with the conducting ion to form a charged complex creating a localized field. This formation of a space charge region influences the transport of the remaining free ions and thus enhances the conductivity. In the case of $AlPO_4$, a reaction as expressed by Eq. (2) is expected to occur. The $AlPO_4$:Li^+ complex

$$AlPO_4 + Li^+ \leftrightarrow AlPO_4{:}\ Li^+ \quad (2)$$

is only stable up to about 27–47 °C. Above the 27–47 °C temperature range, Eq. (2) proceeds towards the left and the beneficial effect of the space charge effect is eliminated.

The exact role of the Li_2O phase is not yet understood, however, it is believed to form a complex similar to that of the dielectric $AlPO_4$ as it is a polar molecule [(Eq. (3))]. Similarly, this complex formation will also contribute to the space charge effect on the transport of the ions. Nevertheless, their individual contribution has yet to be delineated.

$$Li_2O + Li^+ \leftrightarrow Li_2O : Li^+ \quad (3)$$

The activation energies for the sheet specimen corresponding to the low and high temperature regions are 53.1 and 33.8 kJ mol^{-1}, respectively; however, the reported activation energies for a similar glass-ceramic system that showed a linear Arrhenius plot is 36 kJ mol^{-1} [7].

Fig. 5 also shows the total conductivity data for the pelletized specimens prepared using glass-ceramic powder obtained from sheets crystallized at 850 °C for 12 h and sintered at different times (3, 6, 9, and 12 h). The highest conductivity (4.62×10^{-3} S cm^{-1}) at 27 °C is associated with a sintering time of 9 h. The existence of nonlinearity is evident in all the specimens but the inflection point is shifted to a lower temperature (27 °C). The pellet conductivities above the inflection point are lower than the sheet conductivity; however, the conductivity values for the pellet sintered for 9 h below the inflection point matched that of the sheet specimen, although the pellet specimens are supposed to show lower conductivity due to higher grain boundary contribution. This can be attributed to the pellet's higher density and larger grain size.

The low temperature activation energy value ranges from 43.4 to 52.1 kJ mol^{-1} which represents space charge mediated transport of lithium ion conduction [18]. The high temperature activation energy ranges from 29.9 to 31.8 kJ mol^{-1} and characterizes the energy barrier associated with the transport of lithium ion through the crystalline structure of the LAGP. The activation energies of the pellet are slightly lower than the sheet specimen. Furthermore, the high temperature activation energy of the pellet is slightly lower than the bulk activation energy range obtained for $LiGe_2(PO_4)_3$- and Li_2O-doped systems (~37 kJ mol^{-1}) [5].

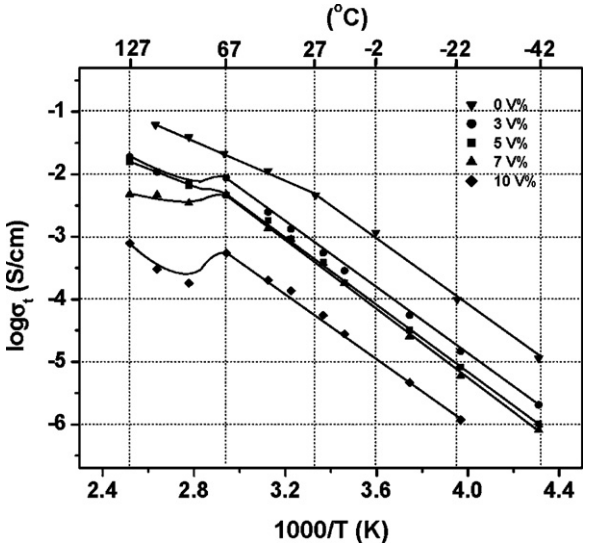

Fig. 6. Arrhenius plots of total conductivity of pelletized LAGP and its composites with different vol% of 0.6BST sintered at 850 °C for 9 h.

Different volume percentages of high dielectric material (0.6BST) were doped to the LAGP glass-ceramic material to study the relationship between the inflection point of the Arrhenius plot of total conductivity and space charge effect. The Arrhenius plots of total conductivity of the pelletized specimens of LAGP glass-ceramic and its composite with 3, 5, 7, and 10 vol% of 0.6BST that were sintered at 850 °C for 9 h are shown in Fig. 6. The sintering of the specimens at 850 °C for 9 h was followed as it gives rise to the highest conductivity for the pelletized specimens. It is observed that the doping of 0.6BST to the LAGP glass-ceramic led to a decrease in conductivity across the entire temperature range, however, the reduction in conductivity varies across the temperature range and also for different doping levels. The inflection point in the Arrhenius plot of total conductivity transformed into a peak of lower intensity for the 3–7 vol% of 0.6BST doping and much stronger peak for the 10 vol% doping accompanied by a shift in the point of inflection from 27 to 64 °C for all doping concentrations. This indicates that the high dielectric phase, 0.6BST, retains the space charge effect up to the high temperature (64 °C). However, the space charge is destroyed beyond this temperature due to the higher thermal energy. In the whole temperature range the decrease in conductivity for the 3–7 vol% doped composite specimens is lower in comparison to the large drop in the case of 10 vol% doping. Apart from achieving a higher inflection point in temperature, the composite specimens with 3–7 vol% doping showed the conductivity to be $\geq 10^{-3}$ S cm^{-1} in the 37–124 °C temperature range.

The LAGP glass-ceramic is a single lithium ion conductor with unity lithium transport number. Its primary transport mechanism involves conduction through the channels of an aluminum germanium phosphate network. Thus, it was anticipated that the addition of 0.6BST would result in reduced conductivities across the entire temperature range due to the blocking effect. From the experimental data presented in Fig. 6, however, it may be inferred that both blocking and space charge effects coexist in the temperature range of −42 to 67 °C.

The nature of adsorption and desorption processes of lithium ion on the dielectric (0.6BST) surface can be investigated by measuring conductivity during heating and cooling cycles. Fig. 7 shows the Arrhenius total conductivity plots of LAGP glass-ceramic specimens doped with 7 vol% 0.6BST during heating and cooling cycles. During the heating cycle, once the lithium ions have been desorbed from

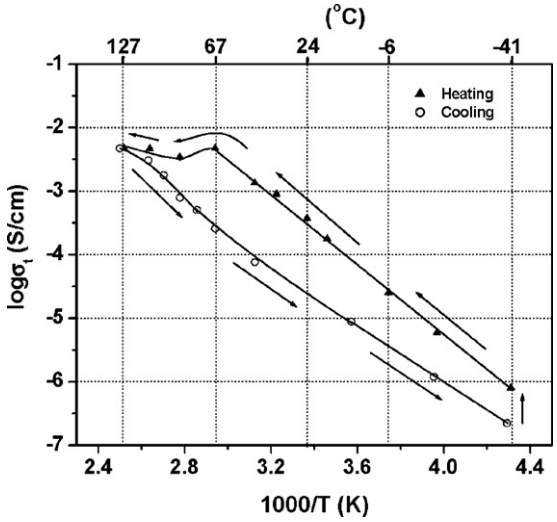

Fig. 7. Arrhenius plot of total conductivity of LAGP-0.6BST (7 vol%) composite specimen during heating and cooling cycles.

the 0.6BST surface above 67 °C, the space charge contribution to conductivity is eliminated. Therefore, the specimens exhibit lower conductivity across the entire temperature range during the cooling cycle. Re-formation of the space charge is a distinct possibility at temperatures lower than the desorption temperature. As seen in Fig. 7, the gap in the Arrhenius total conductivity plot at the lower temperature is narrower which indicates that if the specimen is kept at the low temperature for long enough, space charge will develop and conductivity will retrace to its initial value, but it may take a long time (days). In the case of polymer specimens, it has been shown that the complete recovery of the conductivities at lower temperatures takes from tens to hundreds of hours [20].

4. Conclusion

Lithium aluminium germanium phosphate based superionic conductors and dielectric (0.6BST) material doped specimens were processed and characterized. The lithium ion conductor mainly consists of $Li_{1+x}Al_xGe_{2-x}(PO_4)_3$ ($x = 0.5$) phase with impurities, $AlPO_4$ and Li_2O. The highest conductivity (5.08×10^{-3} S cm^{-1}) at 27 °C was obtained by crystallizing the glass sheet at 850 °C for 12 h. Pelletized specimens prepared from the glass-ceramic powder and sintered at 850 °C for 9 h exhibited a slightly lower conductivity (4.62×10^{-3} S cm^{-1}) at 27 °C. The pellets exhibited slightly enhanced in density and a significant increase in grain size. The interaction of the lithium ion with the impurity phases $AlPO_4$ and Li_2O resulted in the space charge effects that in turn mediated the transport of conducting ions as characterized by a higher activation energy value. This characteristic is attributed to the nonlinearity in the Arrhenius total conductivity plots. The point of inflection in the Arrhenius total conductivity plots has transformed to a peak accompanied by a shift to a higher temperature for the 3–10 vol% dielectric (0.6BST)-doped heterogeneous systems. The peak observed in the doped systems resulted from the influence of the blocking and space charge effects and their co-existence is exhibited in the heterogeneous systems. The conductivity data of thermally cycled specimens supports the concept of adsorption (creation of space charge) and desorption (destruction of space charge or blocking effect) processes of lithium ion on the dielectric (0.6BST) surface by demonstrating that the specimen conductivity at a temperature below 67 °C during the cooling cycle was lower than the heating cycle.

Acknowledgements

The authors acknowledge financial support provided by the Air Force (Contract No. FA8650-06-3-9022) and Meiqing Huang (Wright Patterson Air Force Base, Ohio) and Dale Grant (UDRI) for assistance with the XRD and SEM work.

References

[1] J.M. Tarascon, M. Armand, Nature 414 (2001) 359.
[2] M. Armand, J.M. Tarascon, Nature 451 (2008) 652.
[3] H. Aono, E. Sugimoto, Y. Sadaoka, N. Imanaka, G. Adachi, J. Electrochem. Soc. 136 (1989) 590.
[4] H. Aono, E. Sugimoto, Y. Sadaoka, N. Imanaka, G. Adachi, J. Electrochem. Soc. 137 (1990) 1023.
[5] G. Adachi, N. Imanaka, H. Aono, Adv. Mater. 8 (1996) 127.
[6] J. Fu, Solid State Ionics 96 (1997) 195.
[7] J. Fu, Solid State Ionics 104 (1997) 191.
[8] B.V.R. Chowdari, G.V. Subha Rao, G.Y.H. Lee, Solid State Ionics 136–137 (2000) 1067.
[9] X. Xu, Z. Wen, Z. Gu, X. Xu, Z. Lin, Solid State Ionics 171 (2004) 207.
[10] X. Xu, Z. Wen, X. Yang, J. Zhang, Z. Gu, Solid State Ionics 177 (2006) 2611.
[11] J.S. Thokchom, B. Kumar, Solid State Ionics 177 (2006) 727.
[12] C.J. Leo, B.V.R. Chowdari, G.V. Subha Rao, J.L. Souquet, Mater. Res. Bull. 37 (2002) 1419.
[13] X. Xu, Z. Wen, X. Wu, X. Yang, Z. Gu, J. Am. Ceram. Soc. 90 (2007) 2802.
[14] B. Kumar, C. Chen, C. Varanasi, J.P. Fellner, J. Power Sources 140 (2005) 12.
[15] J.S. Thokchom, C. Chen, K.M. Abraham, B. Kumar, Solid State Ionics 176 (2005) 1887.
[16] B. Kumar, S. Nellutla, J.S. Thokchom, C. Chen, J. Power Sources 160 (2006) 1329.
[17] J. Maier, Prog. Solid State Chem. 23 (1995) 171.
[18] B. Kumar, J.S. Thokchom, J. Amer. Ceram. Soc. 90 (2007) 3323.
[19] B. Kumar, J. Power Sources 179 (2008) 401.
[20] B. Kumar, L.G. Scanlon, Solid State Ionics 124 (1999) 239.